Chaotic transport of particles in two-dimensional periodic potentials driven by ac forces

R. Guantes* and S. Miret-Artés
Instituto de Matemáticas y Física Fundamental, Consejo Superior de Investigaciones Científicas, Serrano, 123, 28006 Madrid, Spain
(Received 5 July 2002; revised manuscript received 23 January 2003; published 21 April 2003)

The diffusive and directed transport of particles in a two-dimensional periodic potential subjected to frictional and time-periodic forces is analyzed in detail. The model represents diffusion of atoms adsorbed on metal surfaces under an applied *ac* electric field (surface electromigration) in the low-temperature limit. The second dimension and the potential energy coupling are shown to play an important role on both diffusion and net currents, depending on the direction of the drive. A properly chosen biharmonic field is able to control the directed ratchetlike dynamics of atoms on *symmetric* surfaces, since current reversals take place by different stabilization of attractors. Reversals identified with hysteresis loops between periodic running attractors are robust against an increase of the second harmonic amplitude, and against temperature effects inside the experimental range for measurements of surface diffusion.

DOI: 10.1103/PhysRevE.67.046212 PACS number(s): 05.45.Ac, 05.60.Cd, 05.40.Fb

I. INTRODUCTION

The problem of transport in periodic potentials concerns different fields in physics, chemistry, and biology [1]. Some of the most significant examples include motion of ions in superionic conductors [2], current-voltage characteristics in Josephson junctions [3] or diffusion of atoms adsorbed on metal surfaces [4]. When noise plays a role on such systems, but the noise intensity (namely, the scaled temperature kT) is much smaller than the barrier height for transport, the conceptual link between these seemingly distinct phenomena can be traced back to Kramers' famous theory of activated escape over a potential barrier [5–7], particularized to periodic potentials. Recently, there has been a renewed interest in this issue due to the recognition that biological molecular motors are able to produce directional motion of cargos along periodic structures [8]. Many different models have been proposed in order to understand their basic physical mechanism of operation [9]. The two necessary ingredients are breaking of detailed balance (the system is driven away from thermal equilibrium due to deterministic or stochastic perturbations) and breaking of spatiotemporal symmetry. The archetypal model reduces to the motion of a particle in a space periodic potential in the presence of friction, stochastic and/or deterministic forces. Out of the many different possibilities to induce directed transport, we will focus on a deterministic time-periodic driving, neglecting in a first approach thermal or stochastic forces, but considering friction and inertial terms. The effect of adding a Gaussian white noise of weak intensity will be studied at the end.

Most of the theoretical models used so far to study transport in periodic potentials under nonequilibrium perturbations have been one dimensional, with a few exceptions [10–15]. Here we will analyze in detail the classical dynamics in two dimensions, say (x,y), with the adiabatic potential being periodic along both directions. Despite the widespread applicability of the model (think of vortex and fluxon motion in superconductors [13,16,17] or separation of macromolecules in 2D devices [18,19]) specific details and parameters of the potential will be particularized to the case of atomic diffusion on metal surfaces under the effect of an ac electric field, a phenomenon known as *surface electromigration* [20–22]. The separability vs nonseparability of this potential will be also discussed, stressing the main qualitative differences, as well as the differences with the one-dimensional case. As a model we take a potential spatially *symmetric* in both dimensions. Therefore, the existence of a net particle current will be eventually due to the *temporal asymmetry* of the time periodic driving. The onset of a stationary flux as we vary a parameter of the system (the driver amplitude) can be then well investigated. Although the denomination *ratchet* is usually reserved for those systems with spatial asymmetry [9], the dynamics exhibited under temporal asymmetry is very similar to that found in underdamped ratchet systems [23–26].

The main purpose of the present paper is a detailed characterization of both the *transport and diffusive* deterministic dynamics of atoms on a low-viscosity metal surface, under additional ac forces of weak and strong amplitudes. The different mechanisms giving rise to directed current will be also analyzed, as well as the existence of multiple *current reversals* which are a common phenomenon in inertial or underdamped ratchets [23–25]. Previous studies of surface electromigration have been restricted to 1D, and have focused on the spatial asymmetry induced in the periodic potential by the Schwoebel barrier at the steps [20,21] or on the jump distributions under weak periodic modulations [22]. Deterministic diffusive transport in a 1D ratchet potential in the *adiabatic* regime has been also studied recently [27].

The classical dynamics of a particle moving on a two-dimensional potential of mean force, with a time periodic driving $F(t)$ of zero average, neglecting thermal effects and interactions with another particles, is described by the couple of equations

$$m\ddot{x} = -\frac{\partial V(x,y)}{\partial x} - \eta\dot{x} + F(t),$$

$$m\ddot{y} = -\frac{\partial V(x,y)}{\partial y} - \eta\dot{y} + \mu F(t), \tag{1}$$

*Electronic address: rgn@imaff.cfmac.csic.es

 ©2003 The American Physical Society

where m is the mass of the particle, the dissipation is supposed to be due to the existence of an Ohmic friction term with friction coefficient $\gamma=\eta/m$, and $\mu\leqslant 1$ is a constant taking into account the projection of the driving force along the x and y directions. The potential $V(x,y)$ representing the adiabatic interaction between an adatom and a periodic substrate symmetric in both directions is taken to be of the form [28,29]

$$V(x,y)=V_0-V_1[\cos(2\pi x/a)+\cos(2\pi y/a)] + V_2\cos(2\pi x/a)\cos(2\pi y/a), \quad (2)$$

where V_0, V_1, and V_2 are constants and a is the period along the x and y directions. By imposing that the potential is zero at the minima, i.e., $V(0,0)=0$, and taking $V(0,\pm a/2)=V_s$ and $V(\pm a/2,\pm a/2)=V_m$, where V_s and V_m are the energies of the saddle points and maxima, respectively (barriers for transport along the parallel directions or the diagonal directions respectively), one obtains the expression

$$V(x,y)=\frac{V_m}{4}+\frac{V_s}{2}-\frac{V_m}{4}[\cos(2\pi x/a)+\cos(2\pi y/a)] + \left(\frac{V_m}{4}-\frac{V_s}{2}\right)\cos(2\pi x/a)\cos(2\pi y/a). \quad (3)$$

The periodic driving is of the form

$$F(t)=E_1\cos(\omega_1 t)+E_2\cos(n\omega_1 t+\phi), \quad (4)$$

with $E_2<E_1$ and n an integer or semi-integer number (harmonic or subharmonic frequency). For $E_2=0$ the equations of motion (1) are unable to produce a net flux of particles in either direction. This is due to symmetry considerations [30]: because equations (1) are invariant with respect to the symmetry transformations $(x,y)\rightarrow(-x,-y)$ and $t\rightarrow t+T_1/2$ $(T_1=2\pi/\omega_1)$ which change the sign of the velocities, running solutions of Eq. (1) with positive and negative velocities along x or y are equally probable, therefore the averaging over possible realizations gives a zero total flux. In order to break the temporal symmetry, we need $E_2\neq 0$ and n an *even* integer number, or a semi-integer. Here we will take a biharmonic driver, $n=2$. Note that in the underdamped limit $\gamma\rightarrow 0$ (Hamiltonian case) the symmetry transformation $t\rightarrow -t+t_0$ also changes the sign of the velocity while leaving the equations of motion invariant for a symmetric driving $F(-t+t_0)=F(t)$, therefore the condition $E_2\neq 0$, $\phi\neq 0,\pi$ is needed to produce a directed current. Moreover, in Hamiltonian systems it has been recently shown that a mixed phase space is necessary in order to observe directed currents [31,32]. It is also worth noting that nonlinear nonadiabatic response to ac fields can be important to explain some rectification mechanisms [33].

Even in one dimension, the consideration of the inertial term and the time periodic force makes the dynamical system nonintegrable [34] giving rise to chaos for certain values of the amplitude E_1 and the driving frequency ω_1. The existence of periodic or chaotic attractors for a given set of initial conditions is related to the presence or not of mode locking between the period of the particle inside the potential well and the period of the external driver T_1 [35]. Therefore, it is convenient to rescale the equations of motion (1) to dimensionless units [24,25] dividing distances by the spatial period a and times by the period of vibration of the particle close to the bottom of the potential well, $T_0=2\pi/\omega_0$, with $\omega_0=2\pi\sqrt{V_s/2ma^2}$.

Then in rescaled units equations (1) read

$$\ddot{x}=-\frac{\partial V(x,y)}{\partial x}-b\dot{x}-f(t),$$

$$\ddot{y}=-\frac{\partial V(x,y)}{\partial y}-b\dot{y}-\mu f(t), \quad (5)$$

with the new friction coefficient $b=\gamma/\omega_0$, and external driver $f(t)=e_1\cos(w_1 t)$ with amplitude $e_1=E_1/ma\omega_0^2=aE_1/2\pi^2V_s$, and frequency $w_1=\omega_1/\omega_0$. The scaled potential $V(x,y)$ is given by

$$V(x,y)=\frac{1}{4\pi^2}\left\{\left(\frac{V_m}{2V_s}+1\right)-\frac{V_m}{2V_s}[\cos(2\pi x)+\cos(2\pi y)] + \left(\frac{V_m}{2V_s}-1\right)\cos(2\pi x)\cos(2\pi y)\right\}. \quad (6)$$

Note that in the scaled potential the barrier for transport along the x or y directions, $V(0,\pm 1/2)$ or $V(\pm 1/2,0)$, is always $1/2\pi^2$, independent of the parameter V_m/V_s. This parameter will modulate the barrier for transport along the diagonal direction, $V(\pm 1/2,\pm 1/2)=V_m/V_s 2\pi^2$, and the strength of the potential coupling. The value $V_m/V_s=2$ gives a separable potential with a cosine shape in each direction. The parameters b and V_m/V_s in the scaled equations are usually dictated by the particular physical system under study, therefore they will be fixed. We will take $b=0.07$ and $V_m/V_s=5/4$ throughout the paper. This particular value of the friction coefficient and maxima to saddle-point ratio has been shown to accurately fit experimental results for self-diffusion of Na atoms on a Cu(001) surface [28], using classical Langevin simulations. We set the scaled frequency w_1 to be of the order of unity. For $w_1\ll 1$, or equivalently $\omega_1\ll\omega_0$, the periodic driver acts adiabatically and its effect is the same to that of a uniform field, while for $w_1\gg 1$ the particle is almost unperturbed since its motion is much slower than the driver variation along a period, which has zero mean value. We choose the value $w_1=0.75$ hereafter.

A common feature of deterministic dissipative and forced periodic systems is the occurrence of broken symmetry, multistability, chaotic behavior, and hysteresis [36]. All these features are present in the one-dimensional case. We remark, however, that for (1D) overdamped systems, where the $\ddot{x}$ dependent term is neglected, chaotic behavior is not possible [34]. A much richer phenomenology regarding the deterministic dynamics is thus present in the underdamped case we study here. In particular, chaotic and hysteretic phenomena are closely related to the existence of current reversals [24,25].

The second driver is used mainly as a perturbation, therefore we will describe first the deterministic dynamics for $e_2=0$. Although a net current of particles is absent in this case due to symmetry, the dynamics presents a large variety of behavior, which is important to analyze for later considerations. Moreover, the main differences with the one-dimensional case and the influence of the potential energy coupling are discussed.

II. DYNAMICS UNDER SYMMETRIC DRIVING

In the absence of forcing ($e_1=0$), trajectories always end up in one of the potential minima because of continuous energy dissipation. When a periodic driving is switched on, particles can gain energy and compensate the energy dissipated. If the net change in energy per forcing period is zero, then the trajectory will describe a periodic motion (limit cycle or periodic attractor). In one dimension, this is given by the condition

$$\int_0^{T_1} \dot{x} e_1 \cos(w_1 t)\,dt = b\int_0^{T_1} \dot{x}^2 dt. \tag{7}$$

Integrating by parts the left-hand side we obtain

$$e_1[x(T_1)-x(0)] = b\overline{v}(E), \tag{8}$$

where $\overline{v}(E)=\int_{-1/2}^{1/2}\sqrt{2[E-V(x)]}dx$ is the average velocity in one spatial period for a particle with energy E. The limit cycles can be locked or oscillating trajectories if they do not have enough energy to surmount the potential barrier [in this case, $x(T_1)=x(0)$ and $\overline{v}(E)=0$ in Eq. (8) above], or running trajectories if they diffuse freely along one direction with positive or negative velocity. Therefore, for weak forcing only small oscillations around the well bottom occur. In order to get running trajectories, E should at least equal the potential energy barrier in Eq. (8). This gives the driver amplitude $e_1=2b/\pi^2\sim 0.015$ in the scaled case.

To obtain a significant picture of the dynamics for a broad range of driver amplitudes, we have plotted bifurcation diagrams in one of the dynamical variables, here the velocity component v_x. That is, we run an ensemble of trajectories with fixed velocities and y coordinate, and values of the x coordinate along one spatial period. Then we plot the v_x variable of each trajectory whenever $t=T_1$ (stroboscopic Poincaré map). This is a proper choice, since periodic attractors are due to synchronization with the driver frequency w_1. Note, that in two dimensions this may not render too much dynamical information, since the v_y component remains unknown. We find, however, that this is mostly determined by the direction of the periodic forcing, i.e., the value of the parameter μ in Eq. (5). Here, and in order to clarify the role of the potential energy coupling in the transport properties, we have studied periodic forcing applied mainly along the x direction ($\mu=10^{-2}$), and forcing along the diagonal ($\mu=1$).

In Fig. 1 we show the bifurcation diagram for the case of $\mu=10^{-2}$, with $e_1\leqslant 0.62$. It turns out that it is qualitatively very similar to the 1D case (not shown here), the main distinctive features will be remarked below. At low values of forcing, only small oscillations along x are seen. For $e_1>0.015$, as predicted by the simple arguments above, a second stable attractor appears, which at the beginning is quasiperiodic and latter becomes periodic. This, however, *does not* correspond to running solutions, but to rotating trajectories (see Fig. 2), which can exceed in amplitude one spatial period as allowed by energy considerations. This makes another important difference with the case of constant forcing (tilted washboard potential) where running solutions always set in above the critical forcing $2b/\pi^2$ [1]. After the attractor with small oscillations becomes unstable for $e_1>0.053$, trajectories which are *transiently* chaotic and running appear, but they eventually converge to the rotating solution. At increasing values of e_1, these chaotic transients can last for very long times, more than 1000 forcing periods. Persistent running solutions appear in our case for $e_1>0.107$ and they are associated with chaotic trajectories, i.e., to a region where frequency locking is absent. This is due to destabilization of a period 3 attractor, which is a common route to chaos in dissipative systems [34]. The first value of the driver amplitude where only *periodic* running solutions exist is $e_1\geqslant 0.15$ [Fig. 1(b)]. Note that in the adiabatic limit $w_1\ll 1$, the effective potential for transport along the x direction $V_{eff}(x,0)=V(x,0)\pm xe_1$ has no minima for $e_1\geqslant 1/2\pi\sim 0.16$ both for positive and negative e_1, therefore one expects purely running solutions close to this value. However, the two running orbits with opposite velocities are equally probable and the net flux is zero. It is important to remark that considering only the adiabatic linear response, a directed current is ruled out by symmetry even when $e_2\neq 0$. One has to go to third order in the response to get a directed current (as a consequence of harmonic mixing) with an asymmetric biharmonic driver [33,37].

As seen from Figs. 1(b)–1(d), chaotic regions alternate with periodic ones. The periodic windows correspond to closed rotating orbits, or to running trajectories, with the possibility of coexistence of both attractors (hysteresis), see for instance the region $0.17<e_1<0.18$ where a period 3 closed orbit coexists with a period 2 running solution. This scheme of chaotic regions with alternating periodic windows of running and rotating orbits is repeated until very high values of the forcing amplitude. With increasing amplitudes, periodic running trajectories tend to be more stable than rotating ones. Here we limit ourselves to analyze the interval $e_1<0.22$, which for some systems is at the edge of the experimental capabilities. For instance, for the parameters of the Cu(001) surface used above, where $a=2.57$ Å, and the barrier for diffusion along x is $V_s=75$ meV, scaled amplitudes of ~ 0.2 correspond to currents of $\sim 10^9$ V m^{-1} that can be achieved in force ion microscopy (FIM) or scanning tunneling microscopy (STM) measurements [21,38]. Note also that we cover mainly the strong field regime $aE_1\gg V_s$ since $aE_1/V_s=1$ for a scaled amplitude $e_1\sim 0.05$

The most prominent distinctive features of the 2D problem as compared with the one-dimensional case, for $\mu=10^{-2}$, is the existence of rotational motions due to the addition of the second dimension, which, however, have their counterparts in oscillating orbits of high amplitudes in the

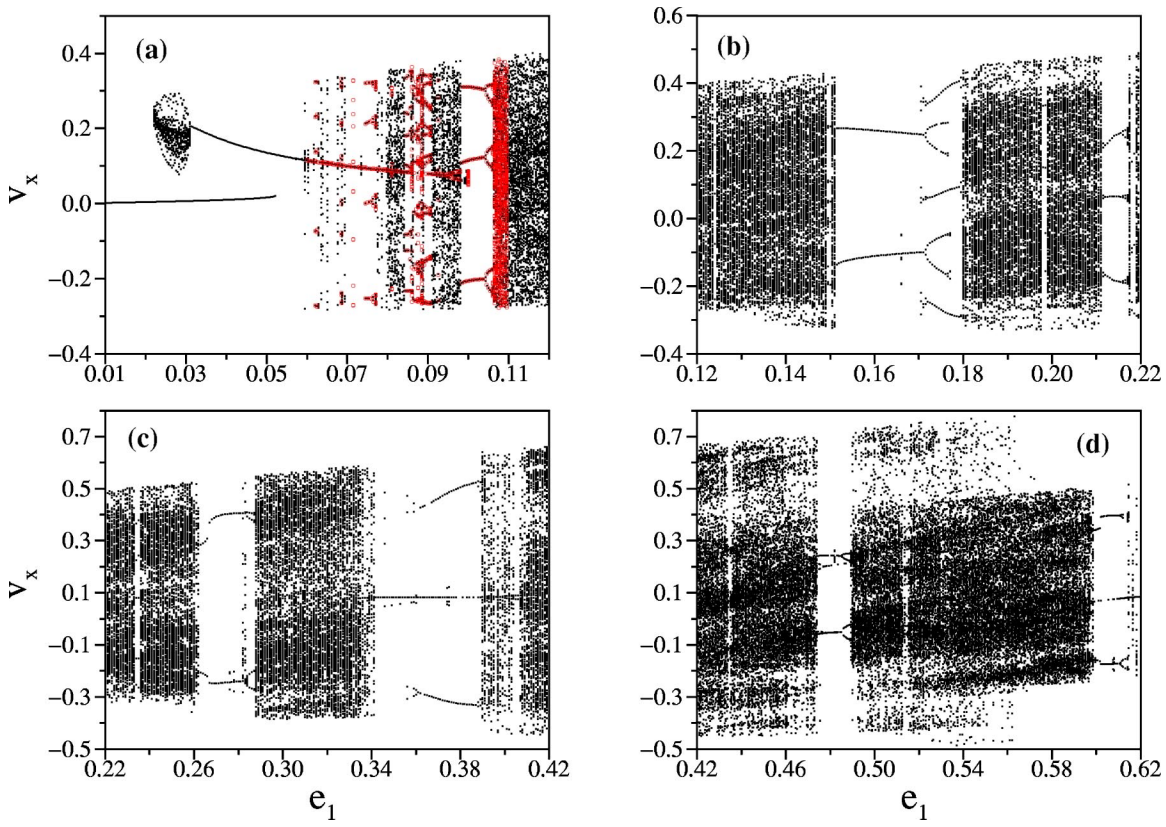

FIG. 1. Bifurcation diagram for the equations of motion (5) with forcing along the x direction ($\mu=10^{-2}$). The (dimensionless) v_x variable is plotted at multiples of the forcing period T_1, after a transient time of 400 T_1. In panel (a) the region $0.6\leqslant e_1\leqslant 0.11$ is also plotted in small red circles after a transient time of $2000T_1$.

1D problem, and the larger destabilization of rotating motions due to the potential energy coupling. For instance, persistent running trajectories appear at higher values ($e_1 \sim 0.114$) of the forcing amplitude compared with the 2D case. We remark that rotational flows embodying several spatial periods have been predicted in 2D periodic potentials [10], but they are generated by a completely different mechanism, namely, by the addition of colored noise, and rotations are there independent of the initial conditions.

If the driver is applied along the diagonal direction, $\mu=1$, a very different dynamical situation takes place (see Fig. 3). The regular intervals of frequency locking are destabilized, and chaos dominates for moderate values of the forcing amplitude (in this case corresponding to running trajectories propagating along the diagonal). At low values of forcing, a period 2 rotating orbit (distorted along the diagonal) appears above the energetically allowed value to surmount the barrier, which is stable until $e_1\sim 0.107$, where it suffers a period doubling cascade to chaos. Transiently chaotic behavior is also observed here for lower values of driving amplitude, but for smaller number of forcing periods compared to the $\mu=10^{-2}$ case. A possible reason for the absence of appreciable intervals of stability of periodic running solutions along the diagonal direction (compare to Fig. 1) can be found if we analyze the Hamiltonian dynamics ($b\rightarrow 0$ limit) without forcing. There one can find the principal periodic orbits for the potential [39] and study its stability as a function of the total energy. For the nonseparable potential (3) the main periodic motions consist of translations along parallel and diagonal directions, see Fig. 4, which are running for energies above the potential barriers, as well as rotating orbits localized in one unit cell in analogy to the forced dissipative case. It turns out that translations along the diagonal direction are very unstable, while those along the parallel directions are much more stable. This instability persists in the forced case.

In the chaotic intervals, dynamical randomness can mimic the behavior of a stochastic system, and transport properties like diffusion can be defined and studied in an analogous way [40]. Statistical quantities of interest are the mean square displacements, from which effective diffusion coefficients along specific directions can be obtained from the generalized Einstein's relation

$$\langle |x(t)-x(0)|^2\rangle = 2D_{eff}t^{1+\alpha}, \quad t\rightarrow\infty \tag{9}$$

as well as velocity power spectra,

$$S(\omega)=\int_{-\infty}^{\infty}\langle \dot{x}(t)\dot{x}(0)\rangle e^{-i\omega t}dt, \tag{10}$$

and jump distributions. The value $\alpha=0$ in Eq. (9) corresponds to the normal diffusive case, analogous to the Brownian motion, while the case $\alpha\neq 0$ implies anomalous transport, superdiffusive ($\alpha>0$) or subdiffusive ($\alpha<0$) [41]. Anomalous (superdiffusive) transport in periodic two-

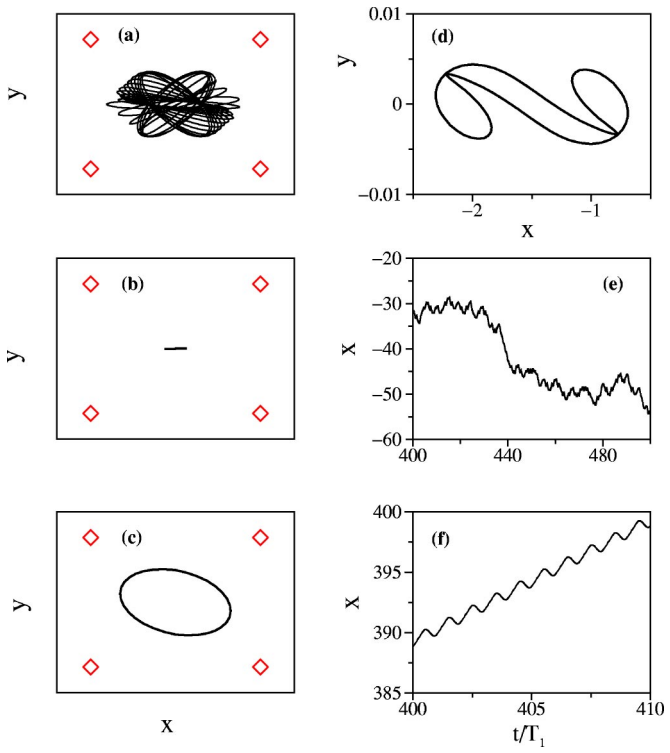

FIG. 2. Some representative attractors appearing at different values of the driver amplitude e_1 (see previous figure). (a) Quasiperiodic attractor at $e_1=0.027$. (b) Coexisting periodic attractor at $e_1=0.027$. (c) Rotating periodic attractor at $e_1=0.04$. (d) Period 3 rotating attractor at $e_1=0.1$. (e) Portion of a running chaotic trajectory at $e_1=0.13$. (f) Running period 1 attractor at $e_1=0.16$. In panels (a)–(c) the maxima of the potential hills delimiting one unit cell are marked with diamonds. In (e)–(f) the time is in units of the stroboscopic period.

dimensional Hamiltonian systems [39,42,43], as well as in circle map models of Josephson junctions [44], has been studied previously. In Hamiltonian ratchets, it has been shown that the current rectification is obtained by desymmetrization of Lévy flights [32,45], which also induce superdiffusion. In a 1D underdamped ratchet system, Mateos [24] observed a superdiffusive growth of the mean square displacement close to a bifurcation point. Here we study in

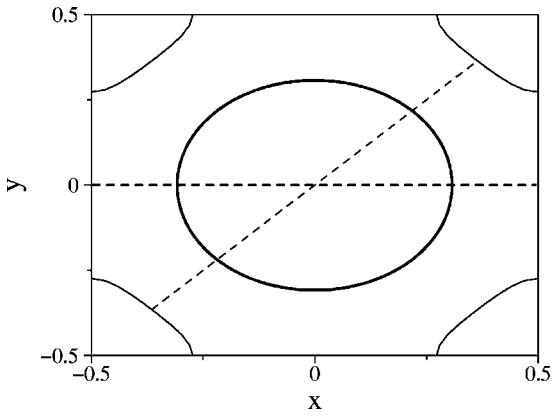

FIG. 4. Main periodic orbits of the Hamiltonian problem with $\gamma=0$ and $e_1=e_2=0$, at a scaled energy of ~ 0.058. This energy is between the barrier for transport along the parallel x or y directions, V_s, and that for transport along the diagonal directions, V_m. The equipotential in one unit cell is plotted to guide the eye. Dashed lines indicate unstable periodic orbits and solid lines indicate stable orbits. For energies above the maxima V_m, the parallel orbit along x becomes stable, while the diagonal orbit is still highly unstable.

detail the diffusive transport *deep* into a chaotic interval, and show that anomalous behavior indeed occurs in this kind of systems at sufficiently long times, under proper forcing amplitudes. This, however, is not related to the occurrence or not of a directed current, both are independent phenomena. We note that the mean square displacement and the velocity autocorrelation function are related at long times by [46]

$$\langle |x(t)-x(0)|^2 \rangle \sim 2t \int_0^t \langle \dot{x}(0)\dot{x}(\tau)\rangle d\tau. \tag{11}$$

By Laplace transforming both sides, one sees that a behavior of the mean square displacement as in Eq. (9) induces a decay of the velocity power spectrum at small frequencies as $\omega^{-\alpha}$ for $\alpha \geqslant 0$. Therefore, an anomalous (superdiffusive) behavior implies an algebraic decay of the velocity power spectrum at small frequencies.

For $\mu=10^{-2}$ and $e_2=0$, we focus on the broad chaotic regions shown in Fig. 1(b), $0.12<e_1<0.15$ and $0.18<e_1<0.21$. For values of the forcing amplitude e_1 deep inside a

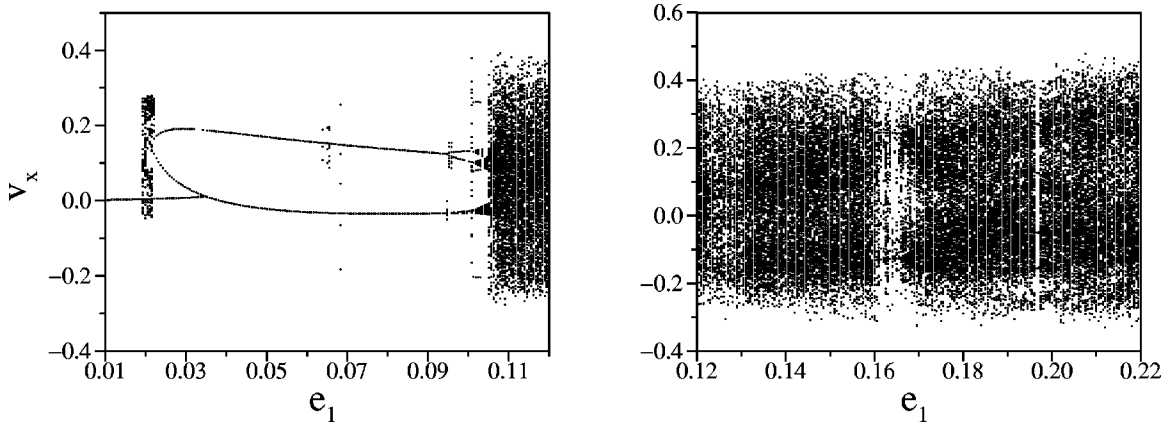

FIG. 3. Bifurcation diagrams for $\mu=1$ (transport along the diagonal direction). The transient time is set equal to $1000T_1$.

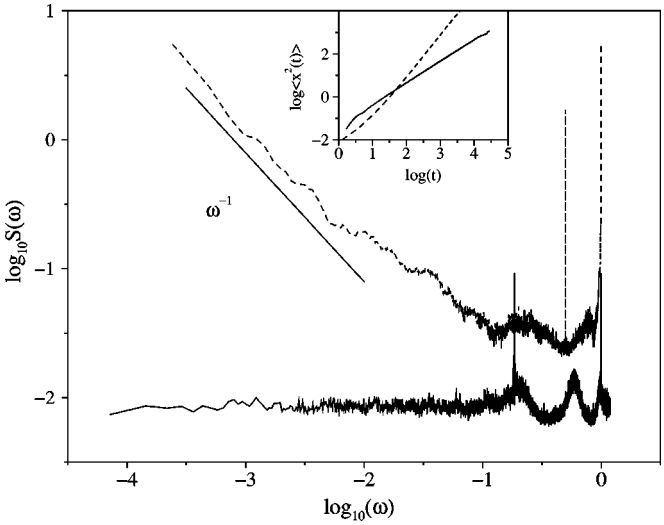

FIG. 5. Velocity power spectrum is at $e_1=0.13$, $e_2=0$. Solid line, $\mu=10^{-2}$. Dashed line, $\mu=1$. The corresponding mean square displacements are shown in the inset. Frequencies are scaled by the driver frequency w_1.

chaotic region, we have observed only a normal diffusive behavior. As an example, we show the velocity power spectrum for $e_1=0.13$ in Fig. 5 (solid line). It converges to a constant value at small frequencies, and the Einstein diffusion coefficient is well defined (the mean square displacement is proportional to t as shown in the inset). The finite frequency part of the spectrum consists of three main peaks at the driver frequency w_1 and two of its harmonics $2w_1$ and $3w_1$ (frequencies in Fig. 5 are scaled by w_1). The sharpest ones correspond to w_1 and $3w_1$. To understand this, we note that $e_1=0.13$ lies between a stable period one running attractor at $e_1\sim 0.15$ and a stable period three rotating attractor at $e_1\sim 0.124$ [small periodicity window in Fig. 1(b)]. Chaotic trajectories in between are made of running pieces in either direction randomly interrupted by small periods of localization, due to the alternative switching between both attractors. The periodic parts give an oscillating contribution to the velocity autocorrelation function, and therefore a series of δ peaks at the fundamental frequencies and its harmonics [47]. The situation can change drastically if the forcing is applied along the diagonal directions. In fact, for the same amplitude $e_1=0.13$, after a very long transient time chaotic trajectories converge to a period 2 attractor. This is illustrated again in Fig. 5 (dashed lines). The mean square displacement behaves as t^2 at long times (inset) and the power spectrum decays as ω^{-1} at small frequencies. We remark that this ballistic behavior is trivial, since all trajectories are periodic and therefore correlated at long times, and should not be confused with ballistic behavior under persistent chaos conditions [44] as we shall show later.

III. ASYMMETRIC BIHARMONIC DRIVING

Here we consider the effect of a biharmonic driving [$n=2$ and $\phi=0$ in Eq. (4)] on the dynamics and on the transport and diffusive properties of the periodic system. As stated above, the most salient feature with respect to the harmonic case is the breaking of the temporal symmetry $F(t)=-F(t+T_1/2)$, thus allowing in principle a net flux of particles along a specific direction for large enough forcing amplitudes. Opposite to the (1D) overdamped case, where a net current is always present after the critical forcing amplitude is reached [with exception of systems with subtle symmetries [30], (b)] here the averaged particle current

$$\langle \mathbf{v}\rangle \equiv \lim_{t\to\infty}\frac{\langle \mathbf{x}(t)-\mathbf{x}(0)\rangle}{t}=\lim_{n\to\infty}\frac{\langle \mathbf{x}(nT_1)-\mathbf{x}(0)\rangle}{nT_1} \qquad (12)$$

can be zero depending on the particular driving amplitudes. A net current for 1D ratchet systems is expected when locking between the driver period and the time required for the particle to cross one unit cell is attained, therefore giving running periodic solutions. Taking as a unit of time the driver period T_1, a running solution of period m in the stroboscopic surface of section will contribute to the flux as $\pm 1/m$, depending on the sign of its velocity, according to Eq. (12). Previous studies of deterministic underdamped ratchets, where the asymmetry was directly in the potential energy function, shown that regular frequency-locked regions always gave rise to a net flux when running solutions were present [25]. Here we show that a net flux can be also observed *deep* in the chaotic (nonlocked) regions, if they are confined between two running periodic attractors. Moreover, the transport properties inside the chaotic regions are also changed by the addition of the second harmonic driver.

In Fig. 6 we plot the bifurcation diagrams for the range of e_1 corresponding to Fig. 1(b), and different values of the biharmonic driver amplitude e_2, from 0.03 (top left) to 0.1 (bottom right) in steps of 0.02. The flux along the x direction is also shown in the upper panels. The desymmetrization of the two period 1 running attractors for $0.15<e_1<0.18$ is seen very clearly. Moreover, for a wide range of values of the parameter e_1 we have an hysteresis loop due to the coexistence of running trajectories in both directions. This induces also a current reversal (from positive to negative net current as we increase e_1), which gradually becomes more steep as desymmetrization is more effective and the hysteresis loop gets narrower. At low biharmonic amplitudes, other smaller current reversals are also seen separated by chaotic regions (between $0.18<e_1<0.22$), corresponding to the narrow periodicity windows inside the chaotic attractors. Therefore, we have two different mechanisms for current reversals: through hysteresis due to different desymmetrization of two running attractors in opposite directions, and through chaotic (no frequency locked) regions between two small locked intervals.

With increasing amplitude e_2, chaos disappears due to stabilization of the running period 1 attractor, and chaos-mediated current reversals seen in Fig. 6(a) also disappear giving rise to overall negative flux. It has been recently noted that a weak *subharmonic* signal could aid to stabilize a directed current in periodically forced ratchets [26]. This is also the case for biharmonic drivers. Which frequency is more effective in stabilizing chaos may depend on the particular system and amplitude range.

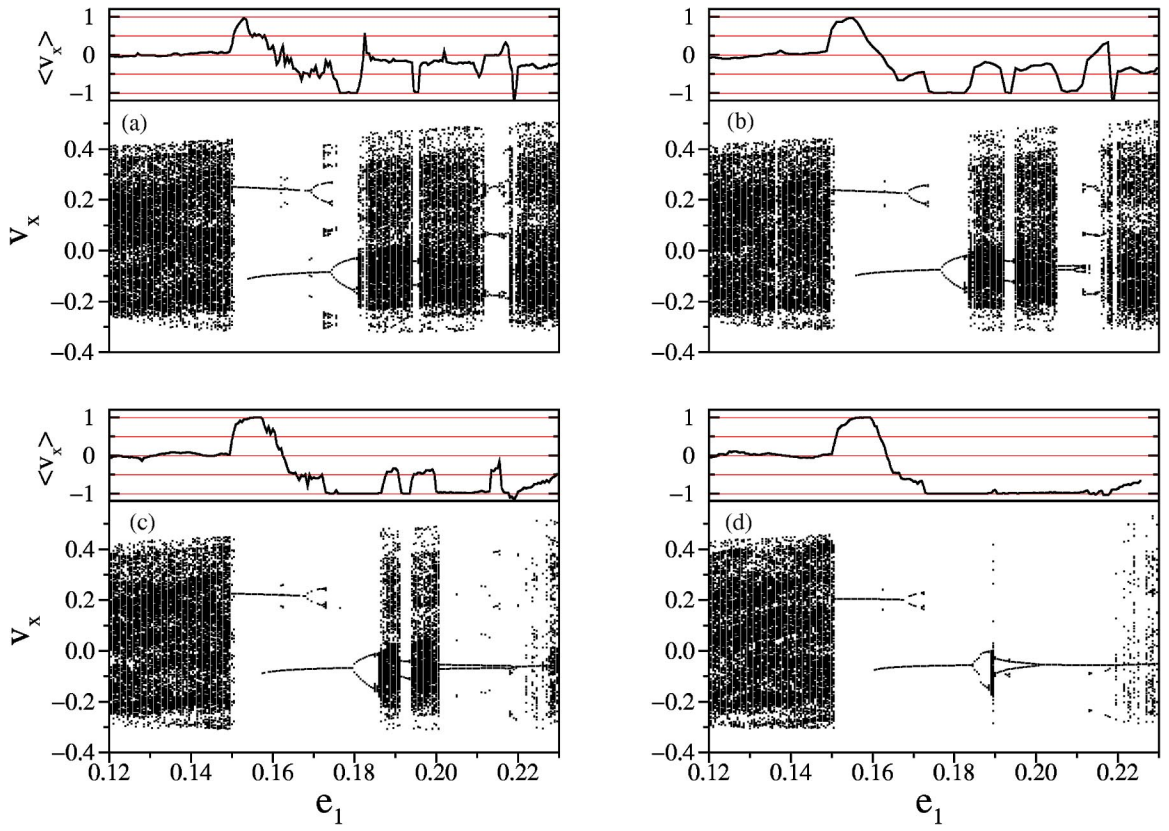

FIG. 6. Bifurcation diagrams and x component of the total flux for $\mu=10^{-2}$ and (a) $e_2=0.03$; (b) $e_2=0.05$; (c) $e_2=0.07$; (d) $e_2=0.1$. The range in e_1 corresponds to that in Fig. 1(b) in all four panels. The flux in the y direction is zero. Grid lines have been plotted at semi-integer values of the flux.

The diffusivelike dynamics deep inside a chaotic interval is also modified by the addition of the harmonic driver. In persistent chaotic regions we found previously ($e_2=0$ case) only normal diffusive behavior with the mean square displacement growing as t. The situation changes when $e_2\neq 0$. As an example, let us examine the case $\mu=10^{-2}$, $e_1=0.13$ analyzed above (see Fig. 5). In Fig. 7 we show the corresponding power spectra and mean square displacements for two moderate values of the harmonic amplitude: $e_2=0.045$ and $e_2=0.055$. An anomalous superdiffusive behavior with exponent $\alpha\sim 0.75$ is seen in both statistical quantities at $e_2=0.045$. The exponent becomes $\alpha\sim 1$ (the $1/f$ noise case) by increasing the value of e_2 (0.055). We remark that in spite of the anomalous diffusive behavior of the chaotic dynamics, the average total flux remains equal to zero. This can be understood if we realize that chaotic trajectories here switch between confined rotating solutions and running ones. The running portions of the chaotic trajectories become longer due to destabilization of the confined solutions (therefore the anomalous growing of the mean square displacement), but both directions are equally probable. A different situation takes place if the chaotic region lies between two running attractors, as is the case for the $0.18<e_1<0.21$ interval in Fig. 6. Here we have detected also $1/f$-noise behavior, due to intermittency [34,48], but now we have long portions of the trajectory running backwards interrupted by random and infrequent bursts where it moves forward for a short time. Now, due to desymmetrization of the backward attractor, the net flux is also negative in the chaotic region.

Finally, let us see the situation when the ac driver is applied along the diagonal direction (Fig. 8). Here the y component of the flux is equal to the x component. One can appreciate that chaos is still more dominant, but a net flux in

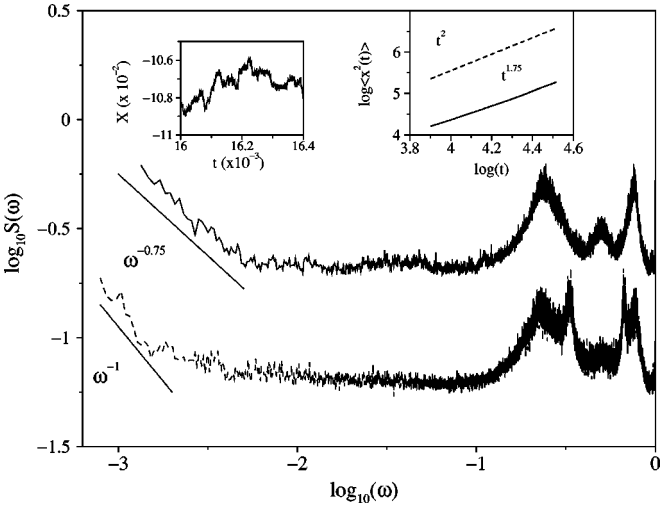

FIG. 7. Velocity power spectra and mean square displacements (inset) for $\mu=10^{-2}$, $e_1=0.13$. Solid line, $e_2=0.045$. Dashed line, $e_2=0.055$. We have also plotted a long time portion of an intermittent chaotic trajectory at $e_2=0.045$ to show the switching between running and localized behavior.

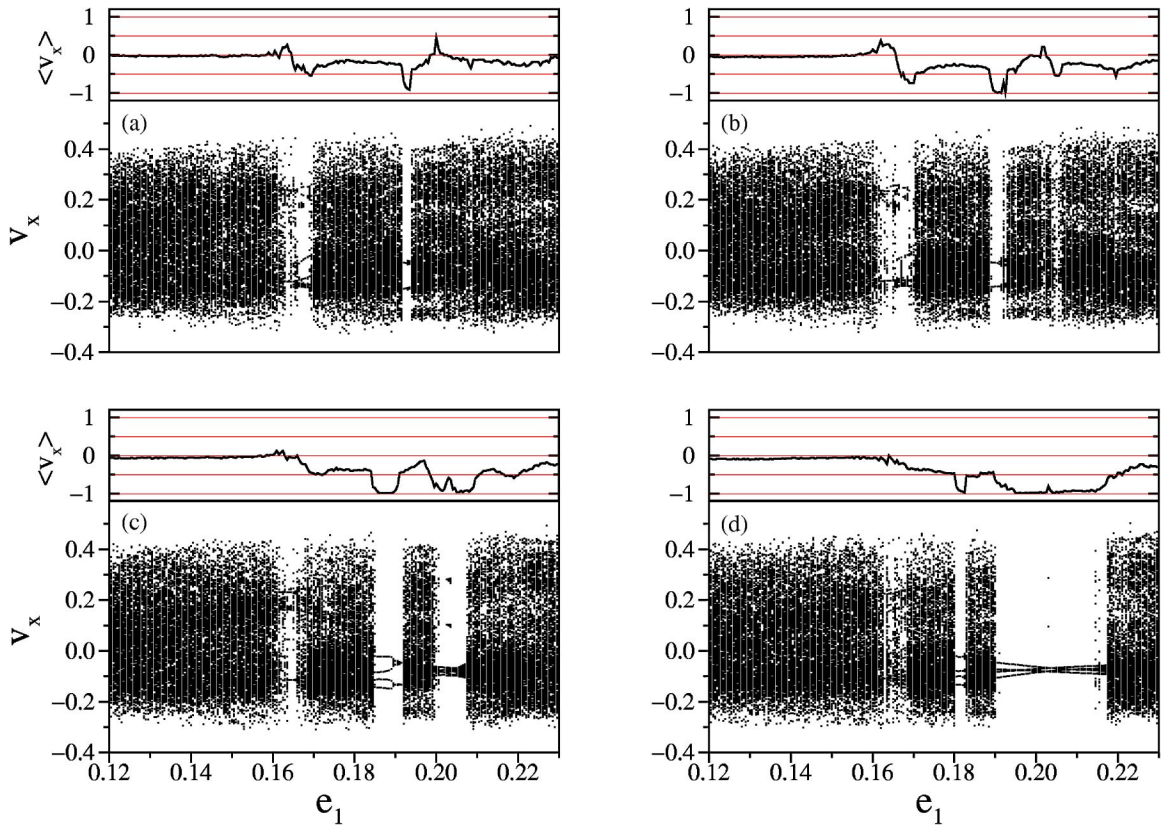

FIG. 8. Same as Fig. 6 for transport along the diagonal direction ($\mu=1$).

chaotic region shows again in between running attractors, and stabilization also takes place.

IV. EFFECT OF NOISE

In many experimental situations a source of noise, due to a finite temperature, is unavoidable. For the particular system and model we are studying here, namely, diffusion of Na atoms on a Cu(001) surface, it has been shown that a Gaussian white noise term properly takes into account the temperature effects on single diffusing adatoms [28,49]. This is justified whenever the vibrational frequencies of the adatoms are lower than the Debye frequency of the substrate. Therefore, we add a noise term $\xi(t)$ to the scaled equations of motion (5), with correlation

$$\langle \xi(t)\xi(t')\rangle = 2b\hat{k}\,\theta\,\delta(t-t'). \tag{13}$$

The scaled temperature is $\hat{k}\,\theta = kT/2\pi^2 V_s$. We keep the temperature low, so that $kT/V_s \ll 1$. The addition of weak noise to a nonlinear dynamical system can modify considerably its local stability properties, but global stability may be relatively conserved [50]. In systems far from equilibrium, it can influence the transport properties and induce transitions between different stable steady states [51]. Since we focused mainly on the strong field regime $E_1 \gg V_s$, or $e_1 \gg 1/2\pi^2$, a weak noise is going to act as a perturbation and it will allow the trajectories to explore larger areas of phase space.

By inspection of the bifurcation diagrams, we found that the structure shown in Figs. 1 and 6 is conserved for temperatures $\hat{k}\,\theta \leqslant 10^{-4}$, which corresponds to just a few kelvin for the parameters of the Na-Cu(001) system. Going to higher temperatures, as the ones employed for instance in experimental measurements of atomic diffusion by Helium-beam scattering techniques [28,49] (50–300 K) one sees that the regular windows observed in Figs. 1 and 6 are blurred, and trajectories can explore the whole phase space due to a frequent escape from the attractors basins. This does not mean, however, that the deterministic dynamics has no influence on the transport properties. Sticking to the attractor basin of regular running orbits is still important at higher temperatures. This can be appreciated in Fig. 9(b), where $\hat{k}\,\theta = 3\times 10^{-3}$ ($T \sim 50$ K). A current reversal is seen to take place at $e_1 \sim 0.16$, which was the value for the deterministic current reversal due to the hysteretic loop between the two running attractors (compare to Fig. 6). It is important to remark that the mechanism for the observed current reversal is only of deterministic nature. In overdamped systems at low forcing amplitudes, the interplay between frequency synchronization and noise can also induce current reversals [52,53].

It is also of interest to study the diffusion properties in the noisy case. Obtaining the effective diffusion coefficient as defined by Eq. (9), we see a normal diffusive behavior until the transition value $e_1 \sim 0.16$, and anomalous diffusion of increasing exponent α with larger forcing amplitudes. This signals again the sticking of stochastic trajectories around the running solutions. For ever spreading trajectories, one can define also a *normal* diffusion coefficient D_{nor} through the second cumulant

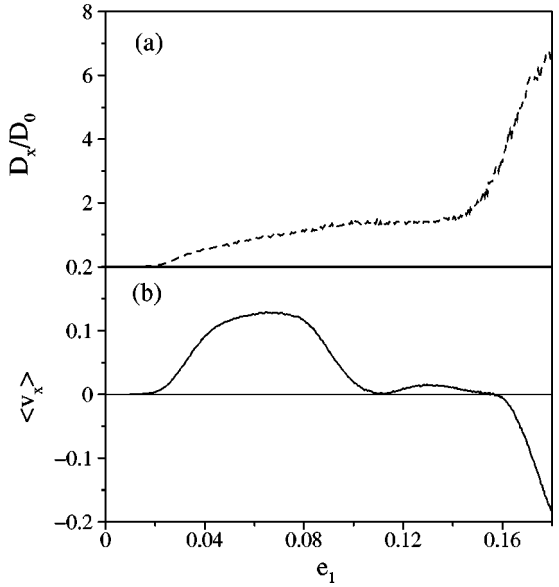

FIG. 9. (a) Normal diffusion coefficient, Eq. (14), along the x direction for $\hat{k}\,\theta \sim 3\times10^{-3}$ and $e_2=0.1$, as a function of the scaled field amplitude e_1 ($\mu=10^{-2}$). (b) Parallel component of the flux for the same parameter values.

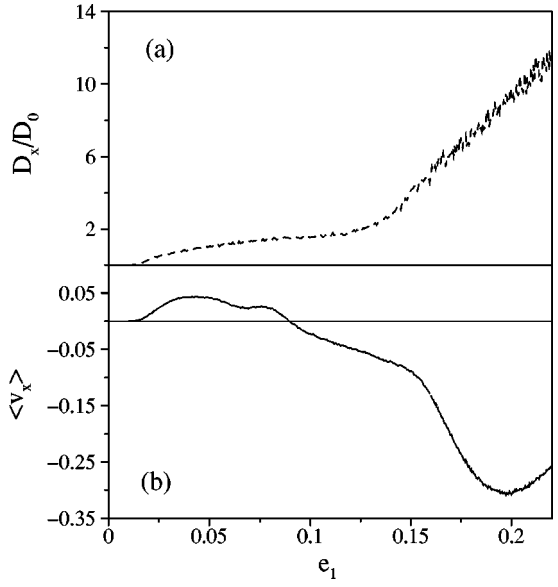

FIG. 10. (a) Normal diffusion coefficient, Eq. (14), along x for the same parameter values are as in Fig. 9 with the electric field applied in the diagonal direction ($\mu=1$). (b) Parallel component of the flux.

$$\lim_{t\to\infty}\langle x^2(t)\rangle-\langle x(t)\rangle^2=2D_{nor}t, \tag{14}$$

which always gives a finite value for D_{nor}. This is plotted in Fig. 9(a), scaled by the Einstein diffusion coefficient $D_0=\hat{k}\,\theta/b$ (free diffusion) at the same parameter values than the flux, $e_2=0.1$ and $T\sim 50$ K (note that at small forcing $e_1 \ll 0.1$ the ac field acts like a *subharmonic* drive). The onset for $D_{nor}\neq 0$ is close to the first threshold value $e_1=2b/\pi^2$, and it reaches a plateau value close to the free diffusion coefficient D_0, until the current reversal takes place at the second threshold value, $e_1=1/2\pi$, where it can be considerably larger than D_0. A similar enhancement of free diffusion close to the threshold value for deterministic running solutions was found in overdamped systems [54].

Applying the field along the diagonal direction ($\mu=1$) gives a different situation for the flux, Fig. 10. Here the current reversal takes place at $e_1\sim 0.09$, which is far away from the adiabatic threshold value for deterministic running solutions along the diagonal, $e_1\sim 0.23$. The reason is that the second frequency component of the drive induces stabilization of periodic running attractors which should be otherwise chaotic, see Fig. 3.

V. CONCLUSIONS

In the present work we have investigated in detail the deterministic dynamics of particles in two-dimensional periodic structures, under the action of frictional and time-periodic forces. Such models are of interest for particle separation in experimental devices [12,18,19] or transport of vortices in superconductors [13], as well as for surface smoothening [20,21] and selective control of self-diffusion on metallic surfaces [22]. Specific parameters have been given to correspond to a semiempirical potential for diffusion of Na atoms on a symmetric Cu(001) surface [28], assisted by ac electric fields.

The two main questions addressed in our study have been the influence of the potential energy coupling on the transport and diffusive dynamics, and the effects induced by addition of a second harmonic field in the transport properties. We have seen that the coupling plays an important role when the time-periodic field is applied along the diagonal, mainly destabilizing running periodic motions, and we have given a qualitative explanation for that in terms of the periodic orbits of the Hamiltonian (force and friction free) case. Under a proper time asymmetric biharmonic driver, coexisting running attractors in opposite directions are desymmetrized, giving rise to directed current and current reversals. A net flux of particles is observed both in the periodic intervals of the field amplitude (frequency locking intervals) as well as in chaotic intervals lying between two running attractors. On increasing the second harmonic amplitude, we observe chaos suppression due to stabilization of a running attractor, and therefore an increase of the interval for which frequency locking is present. The only current reversal that eventually survives is the one produced by an hysteretic loop between two running attractors with opposite velocities. The biharmonic field is also able to induce a drastic cange in the transport properties deep in a chaotic interval, by turning the diffusive motion from normal to anomalous (superdiffusive) and eventually to ballistic ($1/f$ noise) due to intermittency.

Upon the consideration of temperature effects through a Gaussian white noise term, we conclude that features of the deterministic dynamics show up until temperature values inside the experimental capabilities for our specific system. In particular, a current reversal of flux appears close to the threshold value for the onset of pure running solutions. Diffusion is also enhanced with respect to free diffusion around this threshold. The added dimension and the potential energy

coupling play an important role in the noisy case too, since the current reversal appears much earlier when the field is applied along the diagonal direction. These results suggest that an active control of self-diffusion on low-viscosity surfaces is possible by using biharmonic electric fields along specific directions, changing only the amplitude of the first harmonic. New interesting rectification phenomena may occur when two drives are applied along *different* directions, as it has been recently shown [13].

ACKNOWLEDGMENTS

This work was supported in part by DGICYT (Spain) under Contract No. BCM2001-2179. R.G. would like to thank the Minister of Science and Technology (Spain) for a Ramón y Cajal research contract.

[1] H. Risken, *The Fokker-Planck Equation* (Springer, Berlin, 1984), Chap. 11.
[2] P. Fulde, L. Pietronero, W.R. Schneider, and S. Strässler, Phys. Rev. Lett. **35**, 1776 (1975).
[3] A. Barone and G. Paternó, *Physics and Applications of the Josephson Effect* (Wiley, New York, 1982).
[4] J.W.M. Frenken and B.J. Hinch, in *Helium Atom Scattering from Surfaces*, edited by E. Hulpke, Springer Series in Surface Sciences Vol. 27 (Springer-Verlag, New York, 1992), p. 287.
[5] H.A. Kramers, Physica (Utrecht) **7**, 284 (1940).
[6] P. Hänggi, P. Talkner, and M. Borkovec, Rev. Mod. Phys. **62**, 251 (1990).
[7] V.I. Melnikov, Phys. Rep. **209**, 1 (1991).
[8] F. Jülicher, A. Ajdari, and J. Prost, Rev. Mod. Phys. **69**, 1269 (1997); R.D. Astumian, Science **276**, 917 (1997).
[9] P. Reimann, Phys. Rep. **361**, 57 (2002).
[10] A.W. Ghosh and S.V. Khare, Phys. Rev. Lett. **84**, 5243 (2000).
[11] J.D. Bao and Y.Z. Zhuo, Phys. Lett. A **239**, 228 (1998).
[12] (a) M. Kostur and L. Schimansky-Geier, Phys. Lett. A **265**, 337 (2000); (b) M. Bier, M. Kostur, I. Derényi, and R.D. Astumian, Phys. Rev. E **61**, 7184 (2000); (c) I. Derényi and R.D. Astumian, *ibid.* **58**, 7781 (1998).
[13] C. Reichhardt, C.J. Olson, and M.B. Hastings, Phys. Rev. Lett. **89**, 024101 (2002).
[14] R. Eichhorn, P. Reimann, and P. Hänggi, Phys. Rev. Lett. **88**, 190601 (2002).
[15] R. Fleischmann, T. Geisel, and R. Ketzmerick, Phys. Rev. Lett. **68**, 1367 (1992).
[16] K. Harada, O. Kamimura, H. Kasai, T. Matsura, A. Tonomura, and V.V. Moshchalkov, Science **274**, 1167 (1996).
[17] J.F. Wambaugh, C. Reichhardt, C.J. Olson, F. Marchesoni, and F. Nori, Phys. Rev. Lett. **83**, 5106 (1999).
[18] D. Ertas, Phys. Rev. Lett. **80**, 1548 (1998); T.A.J. Duke and R.H. Austin, *ibid.* **80**, 1552 (1998).
[19] C. Kettner, P. Reimann, P. Hänggi, and F. Müller, Phys. Rev. E **61**, 312 (2000).
[20] I. Derényi, C. Lee, and A.L. Barabási, Phys. Rev. Lett. **80**, 1473 (1998).
[21] (a) P.J. Rous, T.L. Einstein, and E.D. Williams, Surf. Sci. **315**, L995 (1994); (b) P.J. de Pablo, J. Colchero, J. Gómez-Herrero, A. Asenjo, M. Luna, P.A. Serena, and A.M. Baró, *ibid.* **464**, 123 (2000).
[22] P. Talkner, E. Hershkovitz, E. Pollak, and P. Hänggi, Surf. Sci. **437**, 198 (1999); M. Borromeo and F. Marchesoni, *ibid.* **465**, L771 (2000).
[23] P. Jung, J.G. Kissner, and P. Hänggi, Phys. Rev. Lett. **76**, 3436 (1996).
[24] J.L. Mateos, Phys. Rev. Lett. **84**, 258 (2000).
[25] M. Barbi and M. Salerno, Phys. Rev. E **62**, 1988 (2000).
[26] M. Barbi and M. Salerno, Phys. Rev. E **63**, 066212 (2001).
[27] M. Borromeo, G. Costantini, and F. Marchesoni, Phys. Rev. E **65**, 041110 (2002).
[28] J. Ellis, A.P. Graham, F. Hofmann, and J.P. Toennies, Phys. Rev. B **63**, 195408 (2001).
[29] G. Caratti, R. Ferrando, R. Spadacini, and G.E. Tommei, Phys. Rev. E **54**, 4708 (1996).
[30] (a) S. Flach, O. Yevtushenko, and Y. Zolotaryuk, Phys. Rev. Lett. **84**, 2358 (2000); (b) P. Reimann, *ibid.* **86**, 4992 (2001).
[31] H. Schanz, M.-F. Otto, R. Ketzmerick, and T. Dittrich, Phys. Rev. Lett. **87**, 070601 (2001).
[32] S. Denisov and S. Flach, Phys. Rev. E **64**, 056236 (2001).
[33] S. Denisov, S. Flach, A.A. Ovchinnikov, O. Yevtushenko, and Y. Zolotaryuk, Phys. Rev. E **66**, 041104 (2002).
[34] E. Ott, *Chaos in Dynamical Systems* (Cambridge University Press, Cambridge, 1993).
[35] D. D'Humieres, M.R. Beasley, B.A. Huberman, and A. Libchaber, Phys. Rev. A **26**, 3483 (1982).
[36] M. Schell, S. Fraser, and R. Kapral, Phys. Rev. A **26**, 504 (1982).
[37] W. Wonneberger, Z. Phys. B: Condens. Matter **53**, 167 (1983).
[38] J.M. Carpinelli and B.S. Swartzentruber, Phys. Rev. B **58**, R13 423 (1998); T.T. Tsong and G. Kellog, *ibid.* **12**, 1343 (1975).
[39] R. Guantes, J.L. Vega, and S. Miret-Artés, Phys. Rev. B **64**, 245415 (2001).
[40] P. Gaspard, *Chaos, Scattering and Statistical Mechanics* (Cambridge University Press, Cambridge, 1998).
[41] R. Metzler and J. Klafter, Phys. Rep. **339**, 1 (2000).
[42] T. Geisel, A. Zacherl, and G. Radons, Phys. Rev. Lett. **59**, 2503 (1987).
[43] J. Klafter and G. Zumofen, Phys. Rev. E **49**, 4873 (1994).
[44] T. Geisel, J. Nierwetberg, and A. Zacherl, Phys. Rev. Lett. **54**, 616 (1985).
[45] S. Denisov, J. Klafter, M. Urbakh, and S. Flach, Physica D **170**, 131 (2002); S. Denisov, J. Klafter, and M. Urbakh, Phys. Rev. E **66**, 046217 (2002).
[46] R. Kubo, T. Toda, and N. Hashitsume, *Statistical Physics II*, edited by P. Fulde, Springer Series in Solid State Sciences (Springer-Verlag, New York, 1991), p. 31.
[47] E. Ben-Jacob, I. Goldhirsch, Y. Imry, and S. Fishman, Phys. Rev. Lett. **49**, 1599 (1982).

[48] A.J. Lichtenberg and M.A. Lieberman, *Regular and Chaotic Dynamics* (Springer-Verlag, New York, 1992).
[49] A.P. Graham, F. Hofmann, J.P. Toennies, L.Y. Chen, and S.C. Ying, Phys. Rev. Lett. **78**, 3900 (1997).
[50] J.P. Crutchfield, J.D. Farmer, and B.A. Huberman, Phys. Rep. **92**, 45 (1982).
[51] P.S. Landa and P.V.E. McClintock, Phys. Rep. **323**, 1 (2000).
[52] R. Bartussek, P. Hänggi, and J.G. Kissner, Europhys. Lett. **28**, 459 (1994).
[53] M. Schreier, P. Reimann, P. Hänggi, and E. Pollak, Europhys. Lett. **44**, 416 (1998); D. Reguera, P. Reimann, P. Hänggi, and J.M. Rubi, *ibid.* **57**, 644 (2002).
[54] P. Reimann, C. Van den Broeck, H. Linke, P. Hänggi, J.M. Rubi, and A. Pérez-Madrid, Phys. Rev. Lett. **87**, 010602 (2001).